

Universality and thermoelectric transport properties of quantum dot systems

D. F. Aranguren-Quintero¹, E. Ramos², J. Silva-Valencia¹, M. S. Figueira³, L. N. Oliveira⁴ and R. Franco¹

¹ *Departamento de Física, Universidad Nacional de Colombia (UNAL), A. A. 5997, Bogotá, Colombia.*

² *División de Ciencias Básicas, Fundación Universidad de América, Bogotá, Colombia.*

³ *Instituto de Física-Universidade Federal Fluminense (IF-UFF),
Av. Litorânea s/n, CEP:24210-346, Niterói, Rio de Janeiro, Brazil.*

⁴ *Instituto de Física de São Carlos-Universidade de São Paulo (IFSC-USP), 369 São Carlos, São Paulo, Brazil.*

(Date: 8 de dezembro de 2020)

We discuss the temperature-dependent thermoelectric transport properties of semiconductor nanostructures comprising a quantum dot coupled to quantum wires: the thermal dependence of the electrical conductance, thermal conductance, and thermopower. We explore the universality of the thermoelectric properties in the temperature range associated with the Kondo crossover. In this thermal range, general arguments indicate that any equilibrium property's temperature dependence should be a universal function of the ratio $T^* = T/T_K$, where T_K is the Kondo temperature.

Considering the particle-hole symmetric, spin-degenerate Anderson model, the zero-bias electrical conductance has already been shown to map linearly onto a universal conductance through a quantum dot embedded or side-coupled to a quantum wire. Employing rigorous renormalization-group arguments, we calculate universal thermoelectric transport coefficients that allow us to extend this result to the thermopower and the thermal conductance. We present numerical renormalization-group results to illustrate the physics in our findings.

Applying the universal thermoelectric coefficients to recent experimental results of the electrical conductance and thermo-voltages versus V_{gate} , at different temperatures in the Kondo regime, we calculate all the thermoelectric properties and obtain simple analytical fitting functions that can be used to predict the experimental results of these properties. However, we cannot check all of them, due to the lack of available experimental results over a broad temperature range.

I. INTRODUCTION

The discovery of the Seebeck and Peltier effects in different metal junctions at the beginning of the 19th century gives rise to a branch of physics called “Thermoelectric”(TE) [1]. Seebeck observed that when two different metals joined together (thermocouple) with the junctions maintained at different temperatures, a voltage difference is generated proportional to the temperature variation between the couple's ends. Some times later, Peltier observed that when an electric current flows through the Seebeck device, heat is either absorbed or rejected depending on the direction of the current along the circuit. Today, the Peltier effect is the basis for many TE refrigeration devices, and the Seebeck effect is the basis for TE power generation devices [2].

Ioffe's prediction in the fifties that doped semiconductors could exhibit relatively large thermoelectric effects [3] had a strong impact on the area of thermoelectric materials. It was followed step by step with the discovery that a thermo-junction between p -type Bi_2Te_3 and bismuth exhibits the maximum temperature difference of 26°C and 40°C between (p - and n -) types Bi_2Te_3 [4]. This compound has dominated the whole field of thermoelectric materials; more specifically, the alloys of Bi_2Te_3 with Sb_2Te_3 for p -type and Bi_2Se_3 for n -type compounds have the highest ZT (see Eq. 7), at around room temperatures, when compared to any other known material [5], and up until now, it is the working material for most Peltier cooling devices and Seebeck thermoelectric generators.

Most state-of-the-art thermoelectric materials have

their dimensionless thermoelectric figure of merit, ZT , in the interval $ZT \simeq [1-2.5]$ (see Fig. 2 of the reference [6]), which is well below the Carnot efficiency [7]. However, the advent of nanotechnology opens up new possibilities for increasing ZT , mainly due to the level quantization and the Coulomb interaction, leading to essential changes in the system's thermoelectric properties. Some promising compounds are the topological insulators (TIs) and Weyl and Dirac's semi-metals, characterized by nontrivial topological orders. The new characteristic of the TIs is that besides the conventional semiconductor bulk band structure, they also exhibit topological surface conduction states. Some of the best thermoelectric materials are also three-dimensional topological insulators, such as Bi_2Te_3 , Bi_2Se_3 , and Sb_2Te_3 [8, 9].

Thermoelectric devices must have at least a $ZT > 3$ in order to attain industrial and household spread; this efficiency has been improved over the years, but it was not attained until now [6]. This is the reason why thermoelectric generators or thermoelectric refrigerators are not part of our daily technology. They are used in particular fields like the satellite and aerospace industry, where the advantages of not having movable parts and not requiring maintenance overshadow the low efficiency [6]. One example of this is the radioisotope thermoelectric generator (RTG) [10], a nuclear electric generator that exploits a radioactive atom's natural decay, usually plutonium dioxide $^{238}PuO_2$, converting, via the Seebeck effect, the heat released by the disintegrated atoms into electricity. Furthermore, in the context of today's climate change, research on new thermoelectric materials that improve thermal efficiency is essential as part of our efforts to

obtain environmentally clean sources of energy.

In this investigation, we focus on studying the semiconductor single-electron transistor (SET), which is the experimental realization of the single impurity Anderson model (SIAM) for finite electronic correlation U . The SIAM was experimentally realized by the Goldhaber-Gordon group [11], with complete control over all of the model's parameters. They measured the electric conductance of a SET and showed its universal character. Recently, interest in studying the thermoelectric properties of the SET has greatly increased and has given rise to several papers that have discuss it, both from the theoretical side [12–20] and from the experimental one [21–27]. A useful review can be found in the references [1, 6, 7].

Universal relations for the thermal dependence of the thermodynamic properties, in the Kondo regime, for the SIAM are well known, and a didactic discussion can be found in Hewson's book [28]. Costi *et al.* [13, 29], showed that in the Kondo limit of the SIAM, the thermoelectric transport coefficients (TTC) are only functions of $T^* = \left(\frac{T}{T_K}\right)$, with the temperature T normalized by the Kondo temperature (T_K). For simplicity, we only use $\left(\frac{T}{T_K}\right)$ in the figures, in the text, we use T^* . They also showed that by employing the NRG, the electric conductance, the temperature normalized thermal conductance, and the thermopower exhibit a universal behavior in the Kondo regime.

The universal behavior of $G(T^*)$ in semiconductor nanostructures was studied in earlier papers [30, 31]. The authors derived an analytical expression that maps the thermal dependence of $G(T^*)$, of a Kondo-asymmetric condition of the SIAM to a universal conductance function $G_S(T^*)$. The corresponding TTC $L_0(T^*)$ (Eq. 27), was calculated by employing the NRG. This analytical mapping is parametrized by T_K and the ground state phase shift $\delta = \frac{\pi n_d}{2}$, which is related to the Friedel's sum rule [28, 32]. For brevity, we call this quantity parameter δ . In this investigation, we derive similar analytical expressions associated with the other TTCs, allowing us to obtain both the thermopower and the thermal conductance in a Kondo asymmetric situation, employing only universal functions derived from the thermal dependence of the symmetric SIAM. Again those analytical functions are parametrized by the Kondo temperature and the parameter δ .

In Sec. II, we define the problem and the model employed in the study of the SET. In Sec. III, we define the thermoelectric properties and their relation with the TTCs. In Sec. IV, we develop the calculations of a mapping between the thermal dependence of the TTCs coefficients in the symmetric limit and the asymmetric condition in the quantum dot's Kondo regime. In Sec. V, we present the results of our research associated with the TTCs and discuss their physical consequences. In Sec. VI, we make a prospect of comparison between our results and the available experimental one. In Sec. VII, we present a summary and the conclusions of this in-

vestigation. In Appendix A, we develop a methodology to apply universal TTCs to experimental thermoelectric properties; we obtained simple analytical fitting functions that can be used to predict these properties' observed behavior.

II. THE HAMILTONIAN FOR THE SET

In this investigation, we extend the previous results obtained for the electrical conductance $G(T^*)$, associated with the TTC $L_0(T^*)$ [12, 13, 30], to all the other TTCs: $L_1(T^*)$ and $L_2(T^*)$. We map the thermal dependence of the TTCs for a Kondo-asymmetric situation as a function of the TTCs for a Kondo-symmetric condition. These mappings are obtained in terms of the renormalized Kondo temperature T^* and the parameter δ .

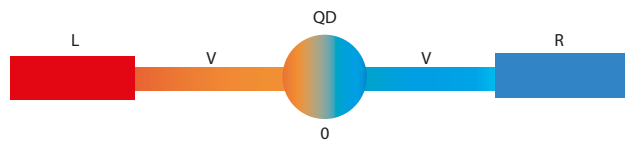


Figure (1) Schematic picture of a semiconductor electron transistor (SET): a quantum dot embedded into conduction leads.

The standard Hamiltonian for the SET studied in this investigation can be written as

$$H = \sum_{\mathbf{k},\sigma} \sum_{\alpha=L,R} E_{\mathbf{k},\sigma}^{\alpha} c_{\mathbf{k},\sigma}^{\alpha\dagger} c_{\mathbf{k},\sigma}^{\alpha} + (E_d n_d + U n_{d\uparrow} n_{d\downarrow}) + \sum_{\alpha=L,R} \sum_{\mathbf{k},\sigma} \frac{V_{\alpha}}{\sqrt{2N}} \left(c_{d\sigma}^{\dagger} c_{\mathbf{k},\sigma}^{\alpha} + c_{\mathbf{k},\sigma}^{\alpha\dagger} c_{d\sigma} \right), \quad (1)$$

where the first term represents the left ($\alpha = L$) and right ($\alpha = R$) leads, characterized by hot and cold free conduction electron (c-electrons) reservoirs, respectively. The quantum dot is embedded in the leads as visually represented in Fig. 1. The second term describes the QD characterized by the local dot energy E_d , and U represents the onsite Coulomb repulsion between the electrons of the QD [33–35]. The third term corresponds to the tunneling between the immersed dot and the left (L) and right (R) semi-infinite leads. The amplitude V_{α} is responsible for the tunneling between the QD and the lead α . For simplicity, we assume symmetric junctions (i.e. $V_{\alpha} = V_L = V_R = V$) and identical leads (i.e. $E_{\mathbf{k},\sigma}^L = E_{\mathbf{k},\sigma}^R = E_{\mathbf{k},\sigma}$) connecting the QD to the quantum wire. The $L(R)$ semi-infinite leads comprise N states $c_{\mathbf{k},\sigma}^L$ ($c_{\mathbf{k},\sigma}^R$) with energies defined by the linear dispersion relation $E_{\mathbf{k},\sigma} = (k - k_F) v_F$ ($0 \leq k \leq 2k_F$) so that the bandwidth is $2D = 2v_F k_F$, with D being the half-width of the conduction band. In all the numerical calculations, we consider the unit of energy to be $D = 1$.

III. THERMOELECTRIC PROPERTIES

We calculated the electrical conductance $G(T)$, the thermal conductance $\kappa_e(T)$ and the thermopower $S(T)$ (Seebeck effect) in terms of the transport coefficients, following the standard textbook derivation [36, 37], and the results are

$$G(T) = e^2 L_o(T), \quad (2)$$

$$\kappa_e(T) = \frac{1}{T} \left(L_2(T) - \frac{L_1^2(T)}{L_o(T)} \right), \quad (3)$$

and

$$S = \left(\frac{-1}{eT} \right) \frac{L_1(T)}{L_o(T)}. \quad (4)$$

To calculate the transport coefficients $L_o(T)$, $L_1(T)$, and $L_2(T)$, we employed the results derived by Dong and X. L. Lei [38]. They considered the particle current and thermal flux formulas, through an interacting QD connected to the leads at different temperatures, within the Keldysh non-equilibrium Green's functions (GF) formalism. The electric and thermoelectric transport coefficients were obtained in the presence of the chemical potential and temperature gradients, with the Onsager relation in the linear regime being automatically satisfied. The transport coefficients are given by

$$L_n(T) = \frac{2}{h} \int \left(-\frac{\partial n_F(\omega, T)}{\partial \omega} \right) \omega^n \tau(\omega, T) d\omega, \quad (5)$$

where $n_F(\epsilon, T) = 1/(1 + e^{(\epsilon - \mu)/k_B T})$ is the Fermi-Dirac distribution, with μ being the chemical potential and the transmittance $\tau(\omega, T)$ is given by

$$\tau(\omega, T) = \pi \Gamma \rho_d(\omega, T), \quad (6)$$

where $\rho_d(\omega, T)$ is the spectral density of the QD and $\Gamma = \pi \rho_c(\mu = 0) V^2$ is the Anderson parameter, which is a measure of the d -level width, and $\rho_c(\omega) = \frac{1}{2D}$ is the flat conduction density of states of the leads.

A useful quantity that indicates the system performance is the thermoelectric dimensionless figure of merit ZT [3], which is given by

$$ZT = \frac{S^2 T G}{\kappa_e}. \quad (7)$$

IV. UNIVERSAL MAPPING: TRANSMISSION COEFFICIENT AND THERMOELECTRIC COEFFICIENTS

Following the reference [30], we introduce the normalized even ($a_{\mathbf{k},\sigma}$) and odd ($b_{\mathbf{k},\sigma}$) operators, in order to exploit the inversion symmetry of the system

$$a_{\mathbf{k},\sigma} = \frac{1}{\sqrt{2}} (c_{\mathbf{k},\sigma}^L + c_{\mathbf{k},\sigma}^R), \quad (8)$$

$$b_{\mathbf{k},\sigma} = \frac{1}{\sqrt{2}} (c_{\mathbf{k},\sigma}^L - c_{\mathbf{k},\sigma}^R). \quad (9)$$

It is convenient to write the Hamiltonian of Eq. 1 on the basis of the new operators ($a_{\mathbf{k},\sigma}$ and $b_{\mathbf{k},\sigma}$), to “split” it into two decoupled pieces $H = H_A + H_B$, with

$$H_A = \sum_{\mathbf{k},\sigma} E_{\mathbf{k},\sigma} a_{\mathbf{k},\sigma}^\dagger a_{\mathbf{k},\sigma} + \sum_{\sigma} V \left(f_0^\dagger c_{d,\sigma} + h.c \right) + (E_d n_d + U n_{d\uparrow} n_{d\downarrow}), \quad (10)$$

where $f_0 = \sum_{\mathbf{k},\sigma} \left(\frac{a_{\mathbf{k},\sigma}}{\sqrt{N}} \right)$, is the traditional NRG shorthand notation, and H_B is given by

$$H_B = \sum_{\mathbf{k},\sigma} E_{\mathbf{k},\sigma} b_{\mathbf{k},\sigma}^\dagger b_{\mathbf{k},\sigma}. \quad (11)$$

The Hamiltonian H_B is quadratic and can be exactly diagonalized and decoupled from the quantum dot. On the contrary, the Hamiltonian H_A “carries” all the correlation effects of the quantum dot and the coupling between it and the conduction band. Due to this, the Hamiltonian H_A is the only one relevant for obtaining the transmittance and the spectral density of states for the quantum dot, and can be written as [30]

$$\rho_d(\omega, T) = \frac{1}{f(\omega, T)} \sum_{mn,\sigma} \frac{e^{-\beta E_m}}{Z(T)} | \langle n | c_{d,\sigma}^\dagger | m \rangle |^2 \delta(E_{mn} - \hbar\omega). \quad (12)$$

Here $|m\rangle$ and $|n\rangle$ are the eigenstates of H_A , with eigenvalues E_m and E_n , respectively, $E_{mn} = E_m - E_n$, and $Z(T)$ is the partition function for the Hamiltonian H_A . The Hamiltonian H_B is not dependent on $c_{d,\sigma}$, $[H_B, c_{d,\sigma}] = 0$, and only the eigenvalues and eigenvectors of H_A are required to obtain $\rho_d(\omega, T)$. On the other hand, to calculate the matrix elements $\langle n | c_{d,\sigma}^\dagger | m \rangle$ in Eq. 16, we evaluate the commutator $[H_A, a_{\mathbf{q},\sigma}]$

$$[H_A, a_{\mathbf{q},\sigma}] = E_{q,\sigma} a_{\mathbf{q},\sigma}^\dagger + \frac{V}{\sqrt{N}} c_{d,\sigma}, \quad (13)$$

and performing the summation over q and σ we obtain

$$[H_A, f_0^\dagger] = \frac{1}{\sqrt{3}} f_1^\dagger + V c_d^\dagger, \quad (14)$$

where

$$f_1 = \sqrt{\frac{3}{N}} \sum_q \left(\frac{E_q}{D} \right) a_q, \quad (15)$$

define a new NRG shorthand notation operator.

Equation 14 permits to relate the matrix elements $\langle n|c_{d,\sigma}^\dagger|m\rangle$ in Eq. 16 with the same matrix elements of the operators f_0 and f_1 ,

$$V \langle m|c_d^\dagger|n\rangle = E_{mn} \langle m|f_0^\dagger|n\rangle - \sqrt{3}D \langle m|f_1^\dagger|n\rangle, \quad (16)$$

and a Schrieffer-Wolff transformation of the Hamiltonian H_A , allows us to write it in the Kondo form [30]

$$H_J = \sum_k E_l g_l^\dagger g_l + J_W \sum_{\mu,\nu} \Phi_{0\mu}^\dagger \sigma_{\mu\nu} \Phi_{0\nu} \cdot \mathbf{S}, \quad (17)$$

where the g_l operators are the eigenoperators of the fixed-point Hamiltonian, associated with the unstable local moment (LM) condition of the Anderson impurity model (see ref. [30] for details). Here, $J_W = 4D \frac{\Gamma U}{\pi|E_d|(E_d+U)} \cos^2 \delta_{LM}$, where δ_{LM} is the quantum scattering phase shift, associated with the LM fixed point, and

$$\Phi_0 = \frac{1}{\sqrt{N}} \sum_l g_l, \quad (18)$$

where in the symmetric condition $\delta_{LM} = 0$ and $\Phi_0 = f_0$.

The second term in the Eq. 17 is responsible, in the Kondo regime, for the evolution from the LM fixed point to a Fermi liquid (FL) fixed point, associated with an antiferromagnetic J_W coupling, characteristic of the Kondo effect. We can define the operator

$$\Phi_1 = \sqrt{\frac{3}{N}} \sum_l \left(\frac{E_l}{D} \right) g_l, \quad (19)$$

in an way analogous to the f_1 operator's definition (Eq. 15). In the symmetric condition $\Phi_1 = f_1$, something similar happens with $\Phi_0 = f_0$.

Eqs. 13 and 16 show the universal character of the product $V \langle m|c_d^\dagger|n\rangle$ in the symmetric point (remember $\Phi_0 = f_0$ and $\Phi_1 = f_1$ in this condition). In order to explore what happens in the asymmetric condition, it is necessary to relate the operators f_0 and f_1 to Φ_0 and Φ_1 , (see Appendix A2 of reference [29]). Substituting Eq. (A21) of the reference [29] in Eq. 16 we obtain

$$\sqrt{\pi\rho\Gamma} \langle m|c_d^\dagger|n\rangle = \alpha_0 \langle m|\Phi_0^\dagger|n\rangle + \alpha_1 \langle m|\Phi_1^\dagger|n\rangle. \quad (20)$$

Performing the substitution of Eq. 20 in Eq. 13, we obtain the localized QD spectral density $\rho_d(\omega, T)$, which can be written as

$$\pi\rho\Gamma\rho_d(\omega, T) = \alpha_0^2\rho_0(\omega, T) + \alpha_1^2\rho_1(\omega, T) + \alpha_0\alpha_1\rho_{(01)}(\omega, T), \quad (21)$$

where $\rho_0(\omega, T)$, $\rho_1(\omega, T)$ and $\rho_{(01)}(\omega, T)$ are universal expressions of the Kondo regime and are given by

$$\rho_j(\omega, T) = \sum_{mn} \frac{e^{-\beta E_m}}{Z(T)f(\omega, T)} |\langle n|\Phi_j|m\rangle|^2 \times \delta(E_{mn} - \hbar\omega), \quad (j = 0, 1), \quad (22)$$

and

$$\rho_{(01)}(\omega, T) = \sum_{mn} \frac{e^{-\beta E_m}}{Z(T)f(\omega, T)} (\langle n|\Phi_0|m\rangle \times \langle n|\Phi_1|m\rangle + c.c.) \delta(E_{mn} - \hbar\omega). \quad (23)$$

Substituting Eq. 21 in Eq. 6, the transmittance at energy $\epsilon = \frac{\hbar\omega}{2\pi}$ and temperature T is given by

$$\tau(\omega, T) = \frac{\alpha_0^2}{\rho} \rho_0(\omega, T) + \frac{\alpha_1^2}{\rho} \rho_1(\omega, T) + \frac{\alpha_0\alpha_1}{\rho} \rho_{(01)}(\omega, T). \quad (24)$$

The universal expressions $\rho_0(\omega, T)$, $\rho_1(\omega, T)$ and $\rho_{(01)}(\omega, T)$ “carry” the thermal dependence of $\tau(\omega, T)$. The important point that should be stressed here is that the transmittance is the key physical quantity that enters the calculations of all the thermoelectric coefficients given by Eq. 5. All the dependence of the parameters of the model is taken into account through the coefficients α_0 and α_1 , given by the reference [30]

$$\alpha_0^2 = \cos^2(\delta), \quad (25)$$

$$\alpha_1^2 = \frac{6}{\pi^2} \sin^2(\delta). \quad (26)$$

Taking into account the result of Eqs. 5 and 24, it is possible to compute the thermal dependence of the linear TTCs as a function of (T^*)

$$L_0(T^*) - \frac{1}{h} = - \left(L_0^S(T^*) - \frac{1}{h} \right) \cos(2\delta), \quad (27)$$

where $L_0^S(T^*)$ is the universal coefficient L_0 in the electron-hole symmetric condition of the model, when $E_d = \frac{-U}{2}$ and $\delta = \frac{\pi n_d}{2}$, with $n_d = 1$. All the thermal dependence of $L_0(T^*)$ is contained in the universal function $L_0^S(T^*)$. The function $\cos(2\delta)$ carries all the parameter dependence apart from temperature T , and is characteristic of the asymmetric conditions for the model ($\delta \neq \frac{\pi}{2}$).

Taking into account that $\mathcal{G}_2(T) = e^2 L_0(T)$, we can write the Eq. 27 in the same form as a result previously obtained in reference [30]

$$G_2(T^*) - \mathcal{G}_2 = - (\mathcal{G}_2^S(T^*) - \mathcal{G}_2) \cos(2\delta), \quad (28)$$

where we also should observe that the $\rho_{(01)}(\omega, T)$ term in Eq. 24, due to particle-hole symmetry arguments, makes

no contribution to the thermoelectric coefficients L_0 [39] and L_2 , but contributes to L_1 , as indicated in Eqs. 29 and 30.

The evaluation of the L_1 coefficient, employing the result for the transmission coefficient (Eq. 24) in Eq. 5 ($n = 1$), and taking into account the parity condition of the integrand, give us

$$L_1(T^*) = L_{(01)}(T^*) \cos(\delta) \sin(\delta), \quad (29)$$

where

$$L_{(01)}(T) = \frac{\sqrt{2}\pi}{h\rho} \int_{-D}^D \epsilon \rho_{(01)}(\epsilon, T) \left(-\frac{\partial f(\epsilon, T)}{\partial \epsilon} \right) d\epsilon, \quad (30)$$

which is an universal function of (T^*) in the symmetric Kondo condition, and contains all the thermal dependence of $L_1(T^*)$.

Finally, employing the result for the transmittance (Eq.24) in Eq. 5 ($n = 2$), we obtain the $L_2(T^*)$ coefficient. Again, we take into account the parity of the integrand

$$\frac{L_2(T^*)}{\left(\frac{k_B T}{T_K}\right)^2} - \frac{\pi^2}{6} = -\cos(2\delta) \left(\frac{L_2^S(T^*)}{\left(\frac{k_B T}{T_K}\right)^2} - \frac{\pi^2}{6} \right). \quad (31)$$

The quantity $\frac{L_2^S(T^*)}{\left(\frac{k_B T}{T_K}\right)^2}$ is a universal function of (T^*) , obtained in terms of $L_2^S(T)$, the coefficient for the symmetric condition of the model. As in the previous cases, all the thermal dependence of Eq. 31 in any asymmetric condition of the model is contained in $\frac{L_2^S(T^*)}{\left(\frac{k_B T}{T_K}\right)^2}$, and all the dependence on the parameters of the model is taken into account through the scattering phase shift factor δ .

V. RESULTS AND DISCUSSION: UNIVERSAL MAPPING

In previous papers, [30, 31, 39, 40] one of us (L. N. Oliveira), argued that it is possible to employ experimental data of electrical conductance $G(T^*)$ to obtain the parameter δ , and with it "check" the validity of the Eq. 27 for the SET. Computations for the case of a side-coupled quantum dot were also considered in references [31, 39, 40], including a comparison with experimental results [39]. In all those previous papers, the numerical calculations were done employing NRG, including the computation of the parameter δ .

The NRG logarithmic discretization parameter employed in the simulations of this work was $\Lambda = 2.25$ and the chemical potential, $\mu = 0.0D$. The Kondo temperature, T_K , for each case was obtained by computing the value of the temperature, where the electrical conductance attains the value $G(T_K) = \frac{G_o}{2} = \frac{e^2}{h}$ [41].

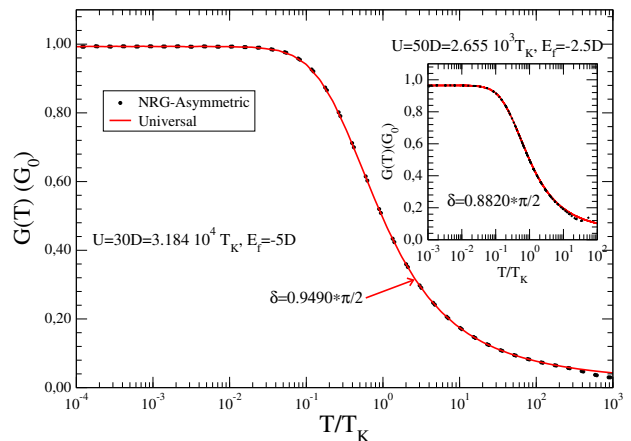


Figure (2) (Color online) The electrical conductance $G(T)$ vs. T^* , corresponding to the Kondo regime. In the inset we show another situation, closer to the crossover between the Kondo and intermediate valence regime.

Fig. 2 shows the results obtained for the electrical conductance $G(T)$ vs. T^* , in units of $G_o = \frac{2e^2}{h}$, in an asymmetric situation employing the results of the symmetrical limit as shown in Fig. 11 of Appendix A. In the main panel, we plot results corresponding to the Kondo regime, employing the following parameters: $E_f = -5.0D$, $U = 30.0D$, with the Kondo temperature being $T_K = 9.422 \cdot 10^{-4}D$. The agreement between the calculated NRG asymmetric results and those obtained employing the NRG symmetric one, the Eq. 27, is notable. The parameter δ computed by the NRG for the asymmetric case is $\delta = 0.9490 \frac{\pi}{2}$, which confirms the validity of Eq. 27 for the SET, previously obtained in reference [30]. In the inset, we plot a situation closer to the crossover transition between the Kondo and intermediate valence regime, with $U = 50.0D$, $E_f = -2.5D$, $T_K = 1.88310^{-2}D$, and $\delta = 0.882 \frac{\pi}{2}$. The agreement obtained is notable for temperatures below $T \simeq 10T_K$, but for temperatures above this value, the results show a small departure from each other, due to the rising of charge fluctuations not being well described by the present treatment.

In Fig. 3, in the main panel, we show the results for $\left(\frac{L_1}{T}\right)$ vs. T^* for the asymmetric Kondo limit, with $E_{QD} = -10.0D$, $U = 30.0D$ and $T_K = 1.517 \cdot 10^{-5}D$. The direct NRG computations are shown by the continuous red line, whereas the results obtained when employing the NRG calculations for the particle-hole symmetric case of the SIAM and Eq. 29 are shown by the black curve. Again, the parameter δ was computed following the same procedure described in the Appendix A. We obtained excellent agreement for a large range of temperatures, between $(10^{-4}T_K \leq T \leq 10^3T_K)$. In the inset, we show the same results, but now for a set of parameters closer to the crossover transition region, between the Kondo and the intermediate valence regimes, with

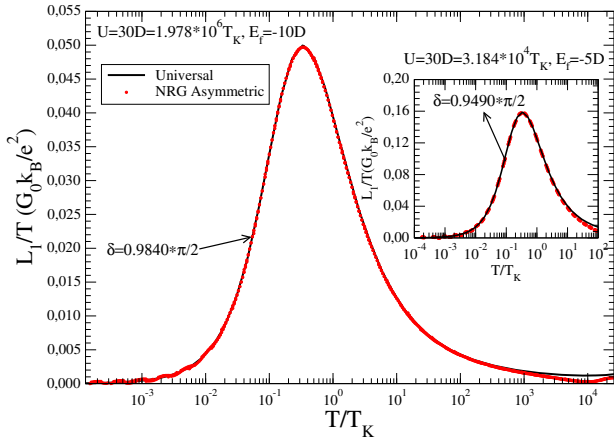


Figure (3) (Color online) Universal thermoelectric coefficient ($\frac{L_1}{T}$), expressed in $\frac{G_0 k_B}{e^2}$ units, vs. T^* for the asymmetric Kondo limit. In the inset, we show the same results for an asymmetric case, in the crossover from an intermediate valence situation to the Kondo limit.

$E_{QD} = -5.0D$, $U = 30.0D$, and $T_K = 9.422.10^{-4}D$.

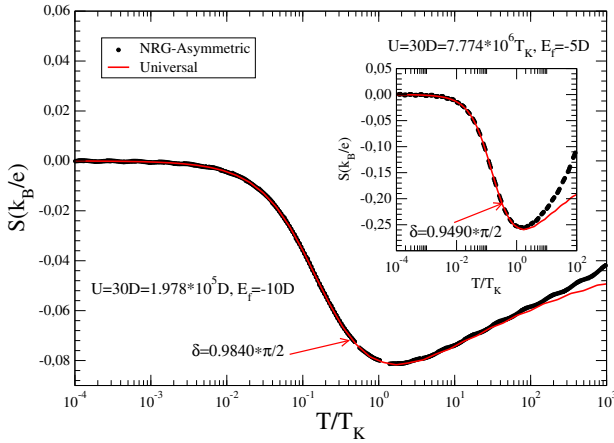


Figure (4) (Color online) Thermopower $S(T^*)$, in $\frac{K_B}{e}$ units vs. T^* . The inset shows the crossover's results from the intermediate valence to the Kondo regime.

In Fig. 4, we plot the thermopower $S(T^*)$ vs. T^* for $E_{QD} = -10.0D$, $U = 30.0D$, and $T_K = 1.517.10^{-5}D$. Employing Eqs. 4, 27, and 29 (red curve), we obtain an excellent agreement between the asymmetric direct NRG results (black curve) and the one employing the symmetric universal TTCs. The minimum at the Kondo temperature manifests the Kondo effect in the thermopower $S(T)$ [13]. There is excellent agreement between both curves up to $T \leq 10^2 T_K$, when charge fluctuations dominate the process. In the inset, we represent a crossover from intermediate valence to the Kondo regime $E_{QD} = -5.0D$, $U = 30.0D$, and $T_K = 9.42210^{-4}D$. Below $T \geq T_K$, the agreement between the two curves is excellent, but above T_K , there is a visible difference between the two results at higher temperatures. We attribute this

difference to the intermediate valence region's proximity, because the present treatment does not describe charge fluctuations well.

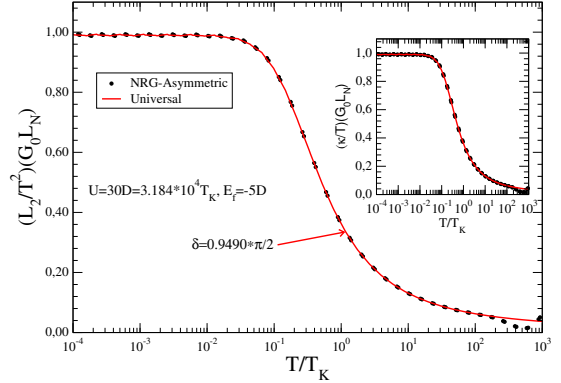


Figure (5) (Color online) Universal thermoelectric coefficient ($\frac{L_2}{T^2}$), in $G_0 L_N$ units, vs. T^* for the asymmetric Kondo limit. The inset shows the temperature-normalized electronic contribution to the thermal conductance ($\frac{\kappa}{T}$) vs. T^* .

In Fig. 5, we plot the results for the universal thermoelectric coefficient for the asymmetric Kondo limit, ($\frac{L_2}{T^2}$) vs. T^* in $G_0 L_N$ units, where $L_N = (\frac{\pi^2}{3})(\frac{k_B}{e})^2$ is the Lorenz number, with $E_{QD} = -5.0D$, $U = 30.0D$, and $T_K = 9.422.10^{-4}D$. Again the agreement between the direct asymmetric NRG results and those achieved employing Eq. 31 and particle-hole symmetric NRG results (fitting presented in Fig. 13) is excellent. In the inset, we show the temperature-normalized electronic contribution to the thermal conductance ($\frac{\kappa}{T}$) vs. T^* . In this case, some small differences appear above $T \geq 30.0T_K$, which is a manifestation of the charge fluctuation process, present in this range of temperatures.

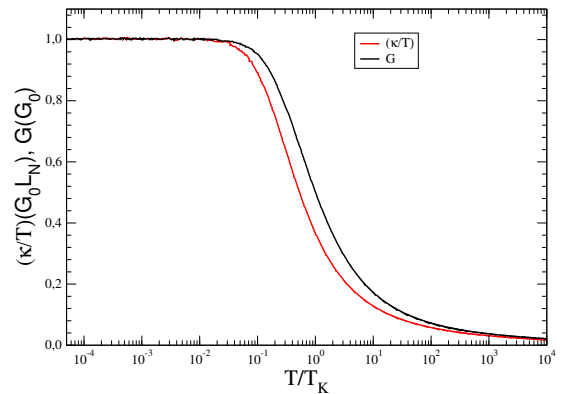


Figure (6) (Color online) Thermal dependence of universal quantities in the symmetric limit. Temperature normalized electronic contribution to the thermal conductance, ($\frac{\kappa(T)}{T}$) ($G_0 L_N$ and the electric conductance $G(T)$) vs. T^* .

Fig. 6 shows the thermal dependence of the universal quantities in the symmetric limit of the SIAM, employing the following parameters: $U = 30.0D$, $E_f = -15.0D$. We plot the temperature normalized electronic contribution to the thermal conductance, $\left(\frac{\kappa(T)}{T}\right)$ and the electric conductance $G(T)$ vs. T^* . The striking similarity of both curves at low temperatures is associated with the Fermi-liquid character of the system and the validity of the Wiedemann-Franz law in this temperature range [12, 13], which leads to the relation $\frac{\kappa(T)}{T} = G(T)$. However, besides the relative closeness of the curves well below and above the Kondo temperature, the two properties are not equal, once the Kondo temperature rules the electrical conductance, whereas the thermal conductance is ruled by a different Kondo scale T_K^θ , as defined in reference [13]

$$\frac{\kappa(T = T_K^\theta)}{T_K^\theta} = \frac{\tilde{\alpha}}{2}, \quad (32)$$

where

$$\tilde{\alpha} = \lim_{T \rightarrow 0} \frac{\kappa(T)}{T}. \quad (33)$$

VI. COMPARISON WITH EXPERIMENTAL RESULTS

In this section, we discuss how to use the methodology employing the universal TTCs to calculate the thermoelectric properties from experimental measurements. In Appendix A, we present a discussion and some examples of applying the universal TTCs methodology to experimental thermoelectric data.

Unfortunately, we did not find experimental SET works in the literature that performed measurements of the electric and thermal conductances and the thermopower in a broad range of temperatures. On the other hand, several papers measured the gate dependence $V_{gate} = V$ of some of these properties for a fixed temperature, T [23, 25, 27, 42, 43]. We focus on applying the universal TTC methodology to the experimental results of the Artis *et al.* paper [25], because they performed several high-quality thermoelectric measurements of Kondo correlated quantum dots (QDs), both below and above the Kondo temperature. They measured the electric conductance $G(T)$, thermocurrent I_{Th} normalized by ΔT (under closed-circuit conditions), and the thermovoltage V_{th} (under open-circuit conditions) as a function of the gate voltage V for a fixed temperature.

Considering an ohmic dependence between the thermovoltage and the thermocurrent in an experimental device, the relation $SG = \alpha \frac{I_{Th}}{\Delta T}$ is valid, where ΔT is the difference of temperatures associated with the Seebeck effect, and where α must be a dimensionless constant for a fixed V_{gate} , but it could be a temperature function. If we assume that at low temperatures $\alpha = \eta T$, with η being a constant that has the inverse of temperature units, we

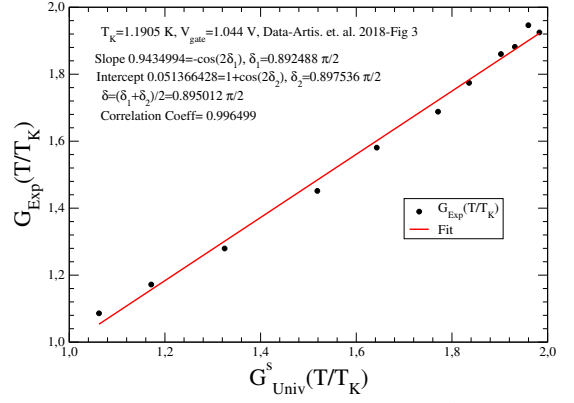


Figure (7) (Color online) $G(T^*)$ vs. $G^S(T^*)$, where the experimental data were obtained from the Artis *et al.* experimental paper [25] with $V_{gate} = 1.044V$ (see Eq. 28).

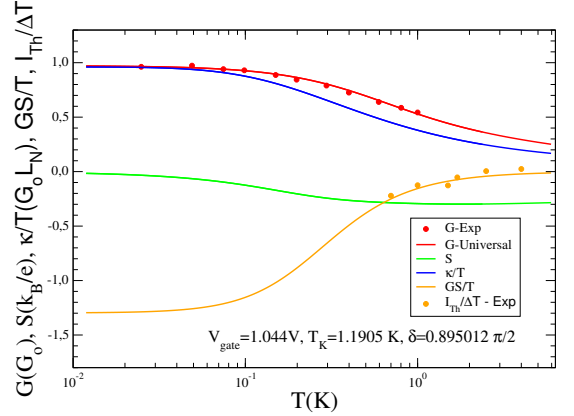


Figure (8) (Color online) Thermoelectric properties as temperature function in Kelvin degrees. The experimental data were obtained from the Artis *et al.* experimental paper [25] with $V_{gate} = 1.044V$.

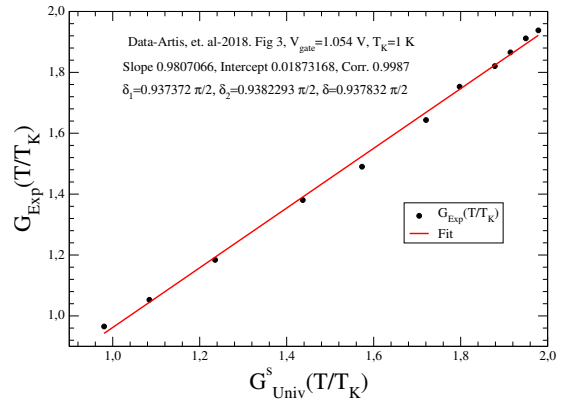


Figure (9) (Color online) $G(T^*)$ vs. $G^S(T^*)$, where the experimental data were obtained from the Artis *et al.* experimental paper [25] with $V_{gate} = 1.054V$ (see Eq. 28).

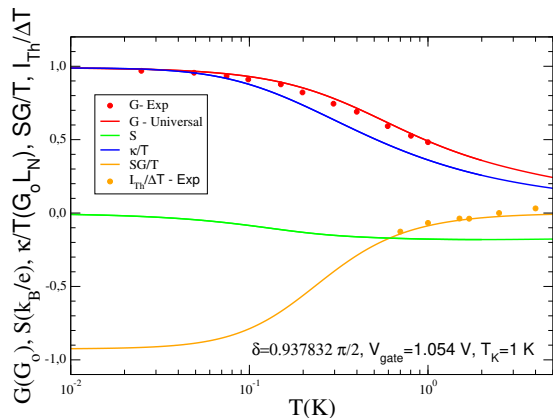


Figure 10 (Color online) Thermoelectric properties as a function of temperature in Kelvin degrees. The experimental data were obtained from the Artis *et al.* experimental paper [25] with $V_{gate} = 1.054V$.

expected that

$$\frac{I_{Th}}{\Delta T} \simeq \frac{SG}{T}. \quad (34)$$

To explore the validity of our predictions, we employed the following results of the Artis *et al.* paper [25]: the data of figures 2b and 3(a,b) for the electrical conductance $G(T)$ at different gate voltages V_{gate} , and the figures 2c and 4a that present the results of $\frac{I_{Th}}{\Delta T}$ as V_{gate} function for different temperatures.

In Figs. 7 and 9, we show the results of the slope and the intercept of the linear figures corresponding to the electrical conductance $G(T)$ of the Artis *et al.* [25] experimental data. We obtained for $V_{gate} = 1.044V$: $\delta = 0.895012\pi/2$ and $T_K = 1.1905K$ and for $V_{gate} = 1.054V$: $\delta = 0.937832\pi/2$ and $T_K = 1.0K$. These Kondo temperatures agree well with the experimental results indicated in Fig. (3b) of the reference [25].

Employing the δ and T_K values obtained, the universal relations for the Onsager coefficients (Eqs. 27-31) and Eqs. 2, 3 and 4, we compute the thermal dependence of the thermoelectric properties: $G(T)$, $S(T)$, $\frac{\kappa}{T}$, and GS/T .

In Fig. 8, we show the results of those properties, corresponding to $V_{gate} = 1.044V$. Initially, we adjust the universal electrical conductance $G_{Universal}$ to the corresponding experimental one, $G - Exp.$, and we compute $\frac{SG}{T}$ and compare it with the experimental data of $\frac{I_{Th}}{\Delta T}$. Unfortunately, the number of experimental data for the $\frac{I_{Th}}{\Delta T}$ in the Artis *et al.* paper is limited, but the agreement of both properties with the available experimental data is excellent. Although there are no available experimental results for the temperature-normalized thermal conductance κ/T and the thermopower $S(T)$, we calculated these properties and obtained fair, reliable results: the κ/T exhibits behavior similar to Fig. 6, and $S(t)$ goes to zero at low temperatures, indicating that the experimen-

tal measurements were performed in a Kondo situation nearer the symmetric limit.

In Fig. 10, we show the same results of Fig. 8, corresponding to $V_{gate} = 1.054V$, and the results show the same overall behavior as the previous one.

VII. CONCLUSIONS

In the present investigation, we employ the NRG treatment to compute the thermal dependence of the TTCs in the Kondo regime. From Eqs. 27-31, we can obtain the thermal dependence of the thermoelectric transport coefficients L_0 , L_1 and L_2 in asymmetric conditions in terms of the Kondo temperature and the parameter δ . All of the thermal dependence is “carried” through the symmetric thermoelectric coefficients’ universal functions of T^* , and all of the dependence on the parameters of the model is taken into account through the parameter δ . We also derived simple universal fitting formulas for the TTCs, given by Eqs. A3, A4, and A5, discussed in the Appendix A, that can be used to predict the thermoelectric properties.

In practical terms, knowledge of the experimental results of the electrical conductance or the thermopower in the Kondo regime at temperature function $\{G(T_i), T_i\}$ or $\{S(T_i), T_i\}$, allows the determination of the Kondo temperature T_K and the parameter δ , and employing the TTCs, we can calculate all the other thermoelectric properties. The ideal situation to “check” our procedure is to obtain all the thermoelectric properties from the experimental measurements, but this requires a consistent and complete set of experimental data for $G(T)$, $S(T)$, and $\kappa(T)$, in a broad temperature range below and above the Kondo temperature, for the same V_{gate} . Unfortunately, we did not find such experimental measurements in the literature, but several papers report measured the gate dependence $V_{gate} = V$ of those properties, for a fixed temperature, T [23, 25, 27, 42, 43].

We focused on applying the universal TTC methodology to the experimental results of the Artis *et al.* paper [25], which measured the electric conductance $G(T)$, thermocurrent I_{Th} normalized by ΔT , and the thermovoltage V_{th} as a function of the gate voltage V for a fixed temperature. We adjusted the experimental results of the $G(T)$ and $I_{Th}/\Delta T$ employing the universal TTCs, obtaining excellent agreement. Although the Artis group did not measure the temperature-normalized thermal conductance κ/T and the thermopower $S(T)$, we calculated those properties, obtaining reliable results.

We expect that this investigation will motivate researchers to carry out experimental work in this direction, in order to compare the procedure expounded here to experimental testing.

ACKNOWLEDGMENTS

We are thankful for the financial support of the Research Division of the Colombia National University, Bogotá (DIB) and the Colombian Scientific Agency - COLCIENCIAS, the São Paulo State Research Foundation (FAPESP), the Brazilian National Research Council (CNPq) and Coordination of Superior Level Staff Improvement (CAPES). E. Ramos acknowledge support from COLCIENCIAS-COLFUTURO doctoral scholarship "Convocatoria Doctorados Nacionales No. 617, 2014-2". R. Franco is grateful for the hospitality of the IFSC-USP-São Carlos and the IF-UFF- Niterói, where part of this work was done.

Apêndice A: Application of the universal TTCs methodology to experimental data

Some earlier papers [30, 31, 39, 40] discussed how to employ experimental data of the thermal dependence of the electric conductance $G(T)$, to calculate the parameter δ to check the validity of Eq. 27. In particular, an almost perfect fit of $G(T)$ with experimental results was found in reference [44]. From the theoretical point of view, it is possible to adjust the experimental results by employing the TTCs in the symmetrical limit of the SIAM obtained from the NRG calculations. Nevertheless, for practical purposes, we can also employ the fitting formulas obtained in Eqs. A3, A4 and A5.

Essentially, the procedure is the following: Given a set of experimental data $[G_i(T_i), T_i]$, choose a trial Kondo temperature T_K , and a new data set $[G_i(T_i^*), T_i^*]$, with $T_i^* = \frac{T_i}{T_K}$ is generated. Since the universal curve for the electric conductance in the symmetric limit of the SIAM, $G^S(T^*)$ vs. T^* is known for the fitting Eq. A3 (Fig. 11), it is possible to obtain the value $G_i^S(T_i^*)$ for each experimental data set of T_i^* , and plot $G_i^S(T_i^*)$ vs. $G_i^S(T_i^*)$. If the plot followed a straight line, the correct Kondo temperature value T_K was attained, and the corresponding parameter δ could be obtained by the slope and the intercept of the straight line (see Eq. 28 and Figs. 7 and 9). On the contrary, if the obtained plot does not follow a straight line, a new trial Kondo temperature T_K must be employed, until a straight line is obtained. Employing Eq. 27 and the fit shown in Eq. A3, it is also possible to compute $L_0(T^*)$.

The same procedure can be performed using the thermopower. Employing Eqs. 4, 27 and 29, it is possible to write the thermopower S as

$$\frac{e}{h}S(T^*) = \frac{\sin(2\delta) \left(\frac{L_{01}^S}{T}\right)(T^*)}{-4\cos^2(\delta) + 2h\cos(2\delta)L_0^S(T^*)}, \quad (\text{A1})$$

which is equivalent to the equation

$$\frac{h \left(\frac{L_{01}^S}{T}\right)(T^*)}{e S(T^*)} = -2\cot(\delta) + 2h\cot(2\delta)L_0^S(T^*). \quad (\text{A2})$$

Given a set of temperatures and a thermopower experimental data set T_i and $S(T_i)$ ($i = 1, \dots, N$) ($[S(T_i), T_i]$), we can choose a tentative Kondo temperature T_K , compute T_i^* , and obtain $[S_i(T_i^*), T_i^*]$. Since we know the universal functions $L_0^S(T_i^*)$ (Fitting of $G_0^S(T_i^*)$ - Eq. A3 associated with Fig. 11) and $\frac{L_{01}^S}{T}(T_i^*)$, it is then a simple matter to compute the fraction on the left-hand side and plot it as a function of $L_0^S(T_i^*)$. If the plot is a straight line, the Kondo temperature has been found. If not, we continue the process until the correct value is attained.

Once the correct parameters δ and T_K are obtained, it is possible to compute $\frac{L_{10}}{T}(T^*)$, employing the universal function $\frac{L_{(10)}}{T}(T^*)$, given by Eq. 29 or the adjusted Eq. A4 of the results shown in Fig. 12. Additionally, it is possible to compute the quantity $\frac{L_2(T^*)}{(k_B T^*)^2}$ by employing Eq. 31, or the fit Eq. A5 of the results shown in Fig. 13. Finally, using Eqs. 2, 3, and 4, we can calculate $G(T^*)$, $S(T^*)$ and $\kappa(T^*)$, and with these, other quantities, such as ZT and the Wiedemann-Franz law.

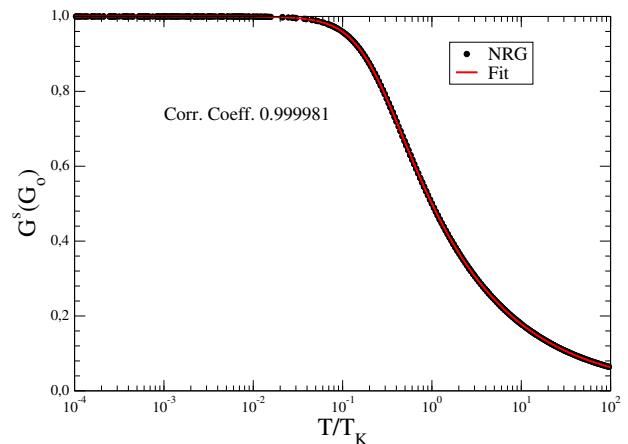


Figura 11 (Color online) NRG Universal electrical conductance $G^S(G_o)$ in the symmetrical limit of the SIAM vs. (T^*) , and its fit to Eq. A3.

In Fig. 11, we plot the NRG universal result [29] for the electrical conductance in the symmetrical limit of the Kondo regime $G^S(T^*)$, employing the following parameters: $U = 30.0D$ and $E_f = -15.0D$. The red line is the fit of the NRG data using a one-parameter equation employed in the reference [41],

$$G(T^*) = \frac{G_o}{[(T^*)^2(2^{1/\xi} - 1) + 1]^\xi}, \quad (\text{A3})$$

to adjust the electrical conductance. The parameter ξ determines the steepness of the decrease in conductance with increasing temperature and provides a good fit to

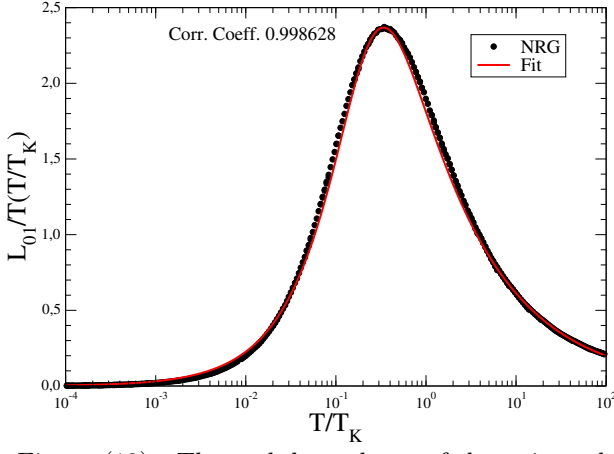


Figure (12) Thermal dependence of the universal function $\left(\frac{L_{(01)}}{T}\right)$ vs. T^* , in the symmetric limit of the SIAM and its fitting to the Eq. A4

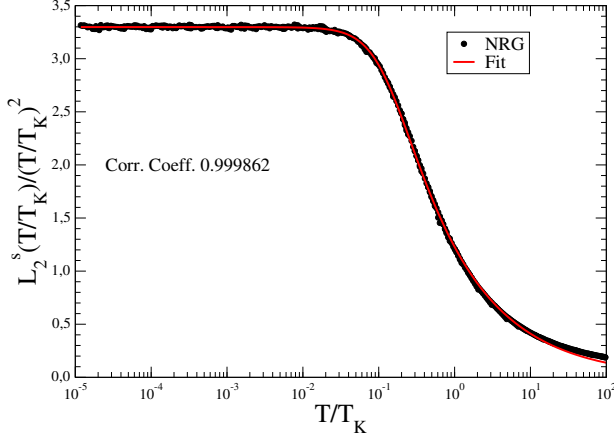


Figure (13) (Color online) The universal quantity $\frac{L_2^S(T^*)}{\left(\frac{k_B T}{T_K}\right)^2}$ vs. T^* , obtained by NRG and its fit to Eq. A5.

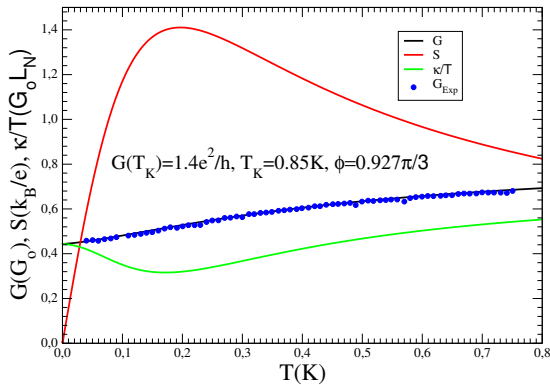


Figure (14) (Color online) Electrical and thermal conductances and thermopower vs. temperature (Kelvin) for a side-coupled SET, obtained from the experimental electrical conductance at $T_K = 0.85\text{K}$ [45].

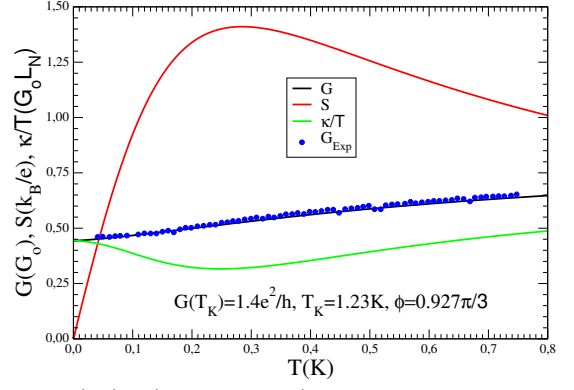


Figure (15) (Color online) Electrical and thermal conductances and thermopower vs. temperature (Kelvin) for a side-coupled SET, obtained from the experimental electrical conductance at $T_K = 1.23\text{K}$ [45].

the numerical renormalization group (NRG) results for the Kondo regime. In our case, $\xi = 0.226022$ and the correlation coefficient = 0.999986. The agreement achieved is excellent. Eq. A3, associated with this fit, allows us to compute the universal TTC $L_0^S(T^*)$ for any T^* value in the range of temperatures presented.

In Fig. 12, we show the thermal dependence of the universal function $\left(\frac{L_{(01)}}{T}\right)(T^*)$ vs. T^* in the symmetric limit of the SIAM, employing the following parameters: $U = 30.0D$ and $E_f = -15.0D$. We obtain good agreement with the universal TTC $\left(\frac{L_{(01)}}{T}\right)(T^*)$ (red line), employing a three-parameter fit expression similar of Eq. A3

$$\left(\frac{L_{(01)}}{T}\right)(T^*) = A_0 \left(\frac{(T^*)^{\frac{A_1}{\xi}}}{(T^*)^2 [A_2^{1/\xi} - 1] + 1} \right)^\xi, \quad (\text{A4})$$

where $A_0 = 11.945007$, $A_1 = 0.860404$, $A_2 = 63.2865$ and $\xi = 0.674506$.

In Fig. 13, we plot the NRG universal results obtained for the TTC $\frac{L_2^S(T^*)}{(k_B T^*)^2}$ in the symmetric limit of the SIAM, employing the following parameters: $U = 30.0D$ and $E_f = -15.0D$. The red line is the fit of the NRG numerical data to Eq. A5; the agreement achieved is excellent. Again, the expression associated with this fit has a form similar to that of Eq. A3

$$\frac{L_2^S}{(T^*)^2} = \frac{A_0}{[(T^*)^2(2^{1/\xi} + A_1) + 1]^\xi}, \quad (\text{A5})$$

where, $A_0 = 3.29776$, $\xi = 0.238365$ and $A_1 = 43.6995$. This formula reduces to Eq. A3 if $A_0 = G_0$ and $A_1 = -1.0$. It also permits computing $\frac{L_2^S(T^*)}{(k_B T^*)^2}$ for any T^* value in the temperature range indicated in the figure.

For completeness, we also repeat earlier calculations employed in the paper [39], which obtained the electrical

conductance and the Kondo temperature using the experimental results of the electrical conductance SET in a side-coupled geometry [45]. We show the results of those calculations in Figs. 14 and 15. The fit of the electri-

cal conductance is excellent. We also calculate $S(T)$ and $\kappa(T)/T$, but we cannot check the reliability of these results, due to the absence of experimental measurements.

-
- [1] D. Sánchez and R. López, *Comptes Rendus Physique* **17**, 1060 (2016).
- [2] T. Tritt, in *Encyclopedia of Materials: Science and Technology*, edited by K. J. Buschow, R. W. Cahn, M. C. Flemings, B. Ilschner, E. J. Kramer, S. Mahajan, and P. Veyssiere (Elsevier, Oxford, 2002) p. 1.
- [3] A. F. Joffe and L. S. Stil, *Reports on Progress in Physics* **22**, 167 (1959).
- [4] D. A. Wright, *Nature* **181**, 834 (1958).
- [5] I. T. Witting, T. C. Chasapis, F. Ricci, M. Peters, N. A. Heinz, G. Hautier, and G. J. Snyder, *Advanced Electronic Materials* **5**, 1800904 (2019).
- [6] J. He and T. M. Tritt, *Science* **357** (2017).
- [7] G. Benenti, G. Casati, K. Saito, and R. Whitney, *Physics Reports* **694**, 1 (2017).
- [8] N. Xu, Y. Xu, and J. Zhu, *npj Quantum Materials* **2**, 51 (2017).
- [9] J. Gooth, G. Schierning, C. Felser, and K. Nielsch, *MRS Bulletin* **43**, 187 (2018).
- [10] M. Zoui, B. S., S. J.G., and B. M., *Energies* **13**, 3606 (2020).
- [11] D. Goldhaber-Gordon, H. Shtrikman, D. Mahalu, D. Abusch-Magder, U. Meirav, and M. A. Kastner, *Nature* **391**, 156 (1998).
- [12] M. Yoshida and L. Oliveira, *Physica B: Condensed Matter* **404**, 3312 (2009).
- [13] T. A. Costi and V. Zlatic, *Phys. Rev. B* **81**, 235127 (2010).
- [14] S. Hershfield, K. A. Muttalib, and B. J. Nartowt, *Phys. Rev. B* **88**, 085426 (2013).
- [15] S. Donsa, S. Andergassen, and K. Held, *Phys. Rev. B* **89**, 125103 (2014).
- [16] V. Talbo, J. Saint-Martin, S. Retailleau, and P. Dollfus, *Scientific Reports* **7**, 14783 (2017).
- [17] T. A. Costi, *Phys. Rev. B* **100**, 161106 (2019).
- [18] T. A. Costi, *Phys. Rev. B* **100**, 155126 (2019).
- [19] Y. Kleorin, H. Thierschmann, H. Buhmann, A. Georges, L. W. Molenkamp, and Y. Meir, *Nature Communications* **10**, 5801 (2019).
- [20] U. Eckern and K. I. Wysokiński, *New Journal of Physics* **22**, 013045 (2020).
- [21] J. P. Heremans, C. M. Thrush, and D. T. Morelli, *Phys. Rev. B* **70**, 115334 (2004).
- [22] R. Scheibner, E. G. Novik, T. Borzenko, M. König, D. Reuter, A. D. Wieck, H. Buhmann, and L. W. Molenkamp, *Phys. Rev. B* **75**, 041301 (2007).
- [23] E. A. Hoffmann, H. A. Nilsson, J. E. Matthews, N. Nakpathomkun, A. I. Persson, L. Samuelson, and H. Linke, *Nano Letters* **9**, 779 (2009).
- [24] N. Hartman, C. Olsen, S. Lüscher, M. Samani, S. Fallahi, G. C. Gardner, M. Manfra, and J. Folk, *Nature Physics* **14**, 1083 (2018).
- [25] A. Svilans, M. Josefsson, A. M. Burke, S. Fahlvik, C. Thelander, H. Linke, and M. Leijnse, *Phys. Rev. Lett.* **121**, 206801 (2018).
- [26] B. Dutta, J. T. Peltonen, D. S. Antonenko, M. Meschke, M. A. Skvortsov, B. Kubala, J. König, C. B. Winkelmann, H. Courtois, and J. P. Pekola, *Phys. Rev. Lett.* **119**, 077701 (2017).
- [27] B. Dutta, D. Majidi, A. García Corral, P. A. Erdman, S. Florens, T. A. Costi, H. Courtois, and C. B. Winkelmann, *Nano Letters* **19**, 506 (2019).
- [28] A. C. Hewson, *The Kondo problem to Heavy Fermions* - Cambridge University Press (1993).
- [29] T. A. Costi, A. C. Hewson, and V. Zlatic, *Journal of Physics: Condensed Matter* **6**, 2519 (1994).
- [30] M. Yoshida, A. C. Seridonio, and L. N. Oliveira, *Phys. Rev. B* **80**, 235317 (2009).
- [31] A. C. Seridonio, M. Yoshida, and L. N. Oliveira, *Phys. Rev. B* **80**, 235318 (2009).
- [32] D. C. Langreth, *Phys. Rev.* **150**, 516 (1966).
- [33] M. Grobis, I. G. Rau, R. M. Potok, H. Shtrikman, and D. Goldhaber-Gordon, *Phys. Rev. Lett.* **100**, 246601 (2008).
- [34] A. V. Kretinin, H. Shtrikman, D. Goldhaber-Gordon, M. Hanl, A. Weichselbaum, J. von Delft, T. Costi, and D. Mahalu, *Phys. Rev. B* **84**, 245316 (2011).
- [35] J. J. Parks, A. R. Champagne, T. A. Costi, W. W. Shum, A. N. Pasupathy, E. Neuscamman, S. Flores-Torres, P. S. Cornaglia, A. A. Aligia, C. A. Balseiro, G. K.-L. Chan, H. D. Abruña, and D. C. Ralph, *Science* **328**, 1370 (2010).
- [36] G. D. Mahan, *Many-Particle Physics* - Springer , 227 (1990).
- [37] J. M. Ziman, *Principles of the Theory of Solids* - Cambridge University Press , 229 (1999).
- [38] B. Dong and X. L. Lei, *Journal of Physics: Condensed Matter* **14**, 11747 (2002).
- [39] A. C. Seridonio, M. Yoshida, and L. N. Oliveira, *EPL (Europhysics Letters)* **86**, 67006 (2009).
- [40] L. N. Oliveira, M. Yoshida, and A. C. Seridonio, *Journal of Physics: Conference Series* **200**, 052020 (2010).
- [41] D. Goldhaber-Gordon, J. Göres, M. A. Kastner, H. Shtrikman, D. Mahalu, and U. Meirav, *Phys. Rev. Lett.* **81**, 5225 (1998).
- [42] R. Scheibner, H. Buhmann, D. Reuter, M. N. Kiselev, and L. W. Molenkamp, *Phys. Rev. Lett.* **95**, 176602 (2005).
- [43] S. F. Svensson, E. A. Hoffmann, N. Nakpathomkun, P. M. Wu, H. Q. Xu, H. A. Nilsson, D. Sánchez, V. Kashcheyevs, and H. Linke, *New Journal of Physics* **15**, 105011 (2013).
- [44] L. Merker, S. Kirchner, E. Muñoz, and T. A. Costi, *Phys. Rev. B* **87**, 165132 (2013).
- [45] M. Sato, H. Aikawa, K. Kobayashi, S. Katsumoto, and Y. Iye, *Phys. Rev. Lett.* **95**, 066801 (2005).